Origins of Solar Systems

Lecture held for the International Max Planck Research School "Solar System and beyond"
February 13-15, 2006

by Klaus Jockers (jockers@mps.mpg.de)

including student lectures by
Clementina Sasso
Lotfi Yelles Chaouche
Ingo von Borstel
Stefan Schröder
Esa Vilenius
Emre Isik
Silvia Protopapa
Elias Roussos

Origin of solar systems: Organization

Lecture (KJ):	Student talks:
Introduction and overview Dense molecular clouds, photo-dissociation regions and protostars	Origin of the elements and Standard Abundance Distribution
Protoplanetary disks Equilibrium condensation of a solar nebula	Agglomeration of planetesimals and protoplanets
Meteorites and the early solar system	Isotope chronology of meteorites and oxygen isotopes
Origin of giant planets	Extrasolar planets
Comets and the early solar system	Transneptunian Objects

Schedule:

Monday und Tuesday: 9:30-12:15 (3*45 Min plus 2*15 Min break)
14:00-16:45
Wednesday: 9:30-12:15

Wednesday afternoon: Seminar and Colloquium

Solar system formation

Early stages (Ewine van Dieshoek, Leiden) a-d

•A lot of steps between d and e:

•Protoplanetary disk is hot near the Sun and cold far from the Sun, condensation of gas depending on temperature

• Formation and growth of planetesimals (strongly dependent on relative velocity)

• Formation of terrestrial and giant planets

• Early Jupiter prevents planetesimal growth in its neighborhood → origin of asteroids

• Comets originate in the Kuiper belt at about 40 AU from the Sun

•Long-period comets are scattered into Oort cloud, disturbed and isotropized by the influence of passing stars and the galactic bulge.

•Short-period comets go directly from Kuiper belt to the inner solar system

•Meteorites come from the surfaces of asteroids and from Mars to the Earth. Their measurement in the laboratory has contributed greatly to our knowledge about solar system formation.

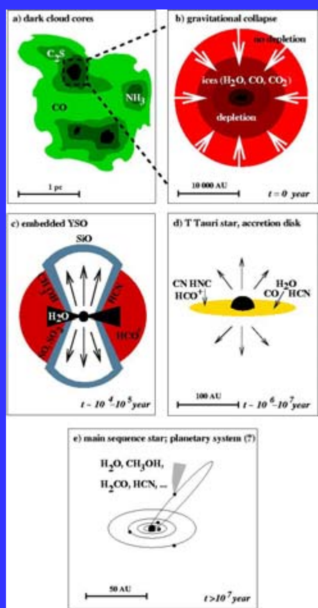

Excurse on blackbody radiation.

Radiation laws related to Planck's law

$$B_\nu(T)d\nu = \frac{2h\nu^3}{c^2}\frac{1}{e^{h\nu/kT}-1}d\nu \quad \text{W m}^{-2}\text{ rad}^{-2}$$

or, using

$$B_\lambda(T)d\lambda = B_\nu(T)d\lambda \cdot c/\lambda^2$$

$$B_\lambda(T)d\lambda = \frac{2hc^2}{\lambda^5}\frac{1}{e^{hc/\lambda kT}-1}d\lambda \quad \text{W m}^{-2}\text{ rad}^{-2}$$

$$\frac{h\nu}{kT} \gg 1 \qquad B_\nu(T) \approx \frac{2h\nu^3}{c^2}e^{-h\nu/kT}d\nu \qquad \text{Wien}$$

$$\frac{h\nu}{kT} \ll 1 \qquad B_\nu(T) \approx \frac{2\nu^2 kT}{c^2} \qquad \text{Rayleigh-Jeans}$$

Wien's displacement law:

$$\frac{c}{\nu_{max}} \cdot T = 5.10 \cdot 10^{-3} \quad \text{[meter K]} \qquad \text{or}$$

$$\lambda_{max} \cdot T = 2.90 \cdot 10^{-3} \quad \text{[meter K]}$$

With T = 290 K (room temperature) we get $\lambda_{max} = 10^{-5}$ m $= 10\,\mu$m.
With T = 5800 K (solar-type star) we get $\lambda_{max} = 0.5\,\mu$m.

Dense molecular clouds,
photodissociation regions and protostars

Excurse: The H_2 molecule

Easily observable: v=1→0 S(1) rotation vibration line at 2.121 μm, T ≈ 2500 K in K band (shock waves)

Note: at the low temperature of dense molecular clouds H_2 does not radiate at all!

In contrast CO: J=1 5.2 K above ground.
CO tracer for H_2
[CO] = 10^{-5} [H_2]

106 F. Combes, Molecules in galaxies at all redshifts, in "The cold universe" Saas-Fee advanced course 32, Springer 2002, pp105-212

$h\nu = hc/\lambda = kT$
$T = hc/k\lambda$
$= 1.439/(\lambda \text{ in cm})$

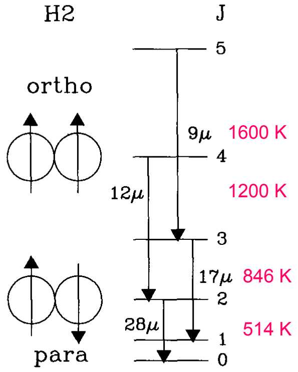

Fig. 1. Schematic of the first levels of the H_2 molecule. The even-J levels are the para-hydrogen, while the odd-J levels are from the ortho-hydrogen. The coupled levels obey $\Delta J = \pm 2$, for quadrupolar transitions, and the two species are not radiatively coupled. The four first rotational lines of hydrogen S(J) (where J is the lower state) are represented – wavelengths in μm, $S(3) = 9$, $S(2) = 12$, $S(1) = 17$ and $S(0) = 28$.

In dense molecular clouds H_2 is most abundant but can form only on grain surfaces.

Different phases of the interstellar medium

Physical Characteristics of Molecular Regions in the Interstellar Medium[a]

	Density (cm^{-3})	T (K)	Mass $M_\odot$	A_V (mag)	Size (pc)	ΔV (km s^{-1})	Examples
Diffuse Clouds	100 – 800	30 – 80	1 – 100	$\lesssim 1$	1 – 5	0.5 – 3	ζ Oph
Translucent Clouds	500 – 5000	15 – 50	3 – 100	1 – 5	0.5 – 5	0.5 – 3	HD 169454; High-latitude clouds
Cold, Dark Clouds							
complex	$10^2 - 10^3$	$\gtrsim 10$	$10^3 - 10^4$	1 – 2	6 – 20	1 – 3	Taurus-Auriga
clouds	$10^2 - 10^4$	$\gtrsim 10$	$10 - 10^3$	2 – 5	0.2 – 4	0.5 – 1.5	B1, B5
cores/clumps	$10^4 - 10^5$	≈ 10	0.3 – 10	5 – 25	0.05 – 0.4	0.2 – 0.4	TMC-1, B335
Giant Molecular Clouds							
complex	100 – 300	15 – 20	$10^5 - 3 \times 10^6$	1 – 2	20 – 80	6 – 15	M 17, Orion
clouds	$10^2 - 10^4$	$\gtrsim 20$	$10^3 - 10^5$	$\gtrsim 2$	3 – 20	3 – 12	Orion OMC-1, W3 A
warm clumps	$10^4 - 10^7$	25 – 70	$1 - 10^3$	5 – 1000	0.05 – 3	1 – 3	M 17 clumps, Orion 1′.5 S
hot cores	$10^7 - 10^9$	100 – 200	$10 - 10^3$	50 – 1000	0.05 – 1	1 – 10	Orion hot core

[a] Table adapted from Goldsmith (1987), Turner (1989*a*) and Friberg and Hjalmarson (1990).

Van Dishoek E.F. et al., in Levy and Lunine eds. "Protostars and Planets III", U. of Az. Press, 1993, pp 163-241.

Van Dishoek E.F. et al., in Levy and Lunine eds. “Protostars and Planets III”, U. of Az. Press, 1993.

TABLE I
Angular Sizes of Protostellar Objects and Capabilities of Telescopes[a]

Linear size	Angular Size				Telescope[b]	Angular Resolution			
	Taurus 140 pc	Orion 450 pc	M17 2.2 kpc	Galactic Center 8.5 kpc		115 GHz	230 GHz	345 GHz	810 GHz
5 AU Inner solar nebula	0″.04	0″.01	—	—	45 m (Nobeyama)	15″	—	—	—
100 AU Outer solar nebula	0″.7	0″.2	0″.05	—	30 m (IRAM)	22″	12″	7″	—
1000 AU Presolar nebula	7″	2″	0″.5	0″.1	15 m (JCMT/SEST)	44″	20″	15″	6″
0.05 pc Cloud core	74″	23″	5″	1″	10 m (CSO)	—	30″	20″	9″
0.5 pc Cloud	12′	4′	50″	12″	Interferometer (OVRO/ BIMA/Nobeyama/IRAM	4–7″	1–2″	—	—

[a] The table only lists the capabilities of currently operating telescopes, not those of future projects.
[b] IRAM = Institute de Radio Astronomie Millimetrique; JCMT = James Clerk Maxwell Telescope; CSO = Caltech Submillimeter Observatory; SEST = Swedish-ESO Submillimetre Telescope; OVRO = Owens Valley Radio Observatory; BIMA = Berkeley-Illinois-Maryland Array.

The Taurus molecular cloud in CO emission.

Note the large extent of the cloud and the many small objects embedded in it.

The map has been done in the light of the CO molecule (millimeter wavelength).

CO is a very important interstellar molecule and believed to be a tracer of the (unobservable) H_2 molecule.

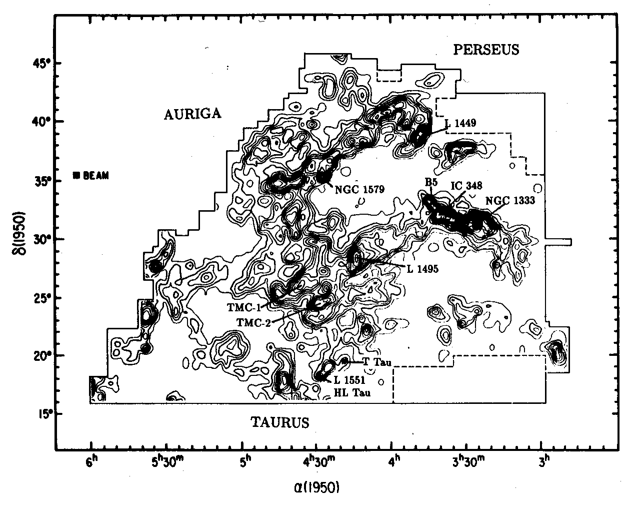

Figure 1. Velocity integrated intensity of CO emission in the Taurus molecular cloud complex. The lowest contour is 0.5 K km s^{-1}, and the separation between contours is 1.5 K km s^{-1}. The border of the surveyed region is indicated by the outer solid line. Various clouds such as B5 and cloud cores such as TMC-1 discussed in the text are indicated (figure adapted from Ungerechts and Thaddeus 1987).

Classes of Chemical Reactions

Type	Process	Rate Coefficient
	Formation Processes	
Radiative association	$X + Y \rightarrow XY + h\nu$	10^{-16}–10^{-9}
Grain surface formation	$X + Y{:}g \rightarrow XY + g$	$\sim 10^{-18}$
	Destruction Processes	
Photodissociation	$XY + h\nu \rightarrow X + Y$	$\sim 10^{-10}$–10^{-8} s^{-1}
Dissociative recombination	$XY^+ + e \rightarrow X + Y$	$\sim 10^{-6}$
Collisional dissociation	$XY + M \rightarrow X + Y + M$	—
	Chemical Processes	
Ion-molecule exchange	$X^+ + YZ \rightarrow XY^+ + Z$	$\sim 10^{-9}$
Charge-transfer	$X^+ + YZ \rightarrow X + YZ^+$	$\sim 10^{-9}$
Neutral-neutral	$X + YZ \rightarrow XY + Z$	$\sim 10^{-12}$

[a] Approximate rate coefficients appropriate for cold dark clouds. All rate coefficients are sensitive to temperature. For photodissociation, the rates in s^{-1} in the unattenuated interstellar radiation field are listed.

Note: minimum two compounds on each side of the reaction equation!

Build-up of complex molecules in dense molecular clouds:

- In dense molecular clouds the only available energy to activate molecules comes from cosmic rays
- Cosmic rays penetrate into molecular clouds up to column densities of 10^{24} cm^{-2}.
- Cosmic rays ionize He and H_2 at rates 10^{-17} to 10^{-16} s^{-1}.
- H_3^+ is formed: $H_2 + H_2^+ \rightarrow H_3^+ + H$ or $H_2 + He^+ \rightarrow H_3^+ + H + He$.

H_3^+ is an interesting “floppy” ring molecule. It has transitions in the L and K bands. It was first discovered on Jupiter, and in the 90th was finally discovered in the interstellar medium.

H_3^+ is the key to molecule formation in dark clouds.

Reactions with O.

→ exothermal

Similar reactions are possible with C. (next slide)

N reactions must proceed in a different way as $N + H_3^+ \rightarrow NH^+ + H_2$ is endothermic. N^+ must be formed first.

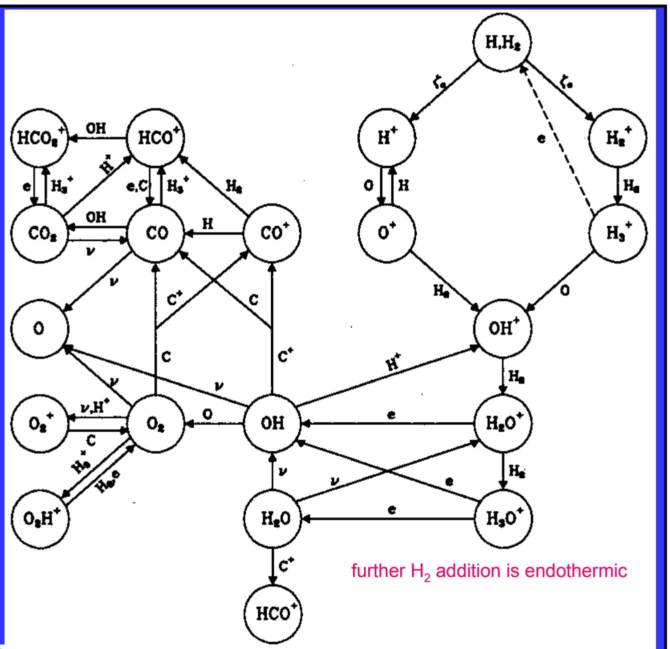

Figure A1. The most important interstellar chemical reactions involving oxygen-bearing molecules (figure from van Dishoeck 1988*a*).

Reactions with C

$CH_3 + C_4H_2 \rightarrow C_5H_3^+ + H_2$
$C_3H^+ + H_2 \rightarrow C_3H_3^+ + h\nu$

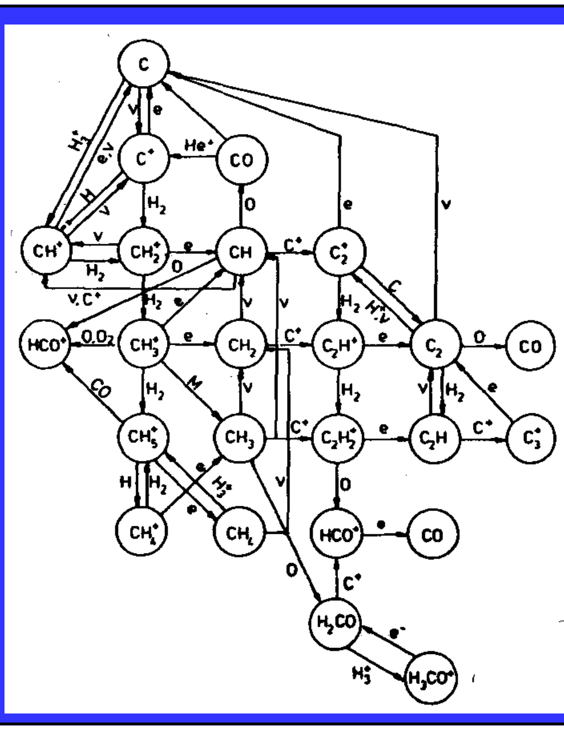

Van Dishoek E.F. et al., in Levy and Lunine eds. “Protostars and Planets III”, U. of Az. Press, 1993.

TABLE III

Identified Interstellar and Circumstellar Molecules[a]

Species	Name	Species	Name	Species	Name
H_2	molecular hydrogen	C_2H_2	acetylene	C_6H	
C_2	diatomic carbon	C_3H	propynylidyne (*l* and *c*)	CH_2CHCN	vinyl cyanide
CH	methylidyne	H_2CO	formaldehyde	CH_3C_2H	methylacetylene
CH^+	methylidyne ion	NH_3	ammonia	CH_3CHO	acetaldehyde
CN	cyanogen	HNCO	isocyanic acid	CH_3NH_2	methylamine
CO	carbon monoxide	$HOCO^+$	protonated carbon dioxide	HC_5N	cyanodiacetylene
CS	carbon monosulfide	$HCNH^+$	protonated hydrogen cyanide		
OH	hydroxyl	HNCS	isothiocyanic acid		
HCl	hydrogen chloride	C_3N	cyanoethynyl	$HCOOCH_3$	methyl formate
NO	nitric oxide	C_3O	tricarbon monoxide	CH_3C_3N	methylcyanoacetylene
NS	nitrogen sulfide	H_2CS	thioformaldehyde	CH_3C_4H	methyldiacetylene
SiC	silicon carbide*	H_3O^+	hydronium ion	CH_3CH_3O	dimethyl ether
SiO	silicon monoxide	C_3S		CH_3CH_2CN	ethyl cyanide
SiS	silicon sulfide	HC_2N		CH_3CH_2OH	ethanol
SO	sulfur monoxide			HC_7N	cyanohexatriyne
PN					
CP	*	C_4H	butadiynyl		
SO^+	sulfoxide ion	C_3H_2	cyclopropenylidene	CH_3C_4CN	
NaCl	sodium chloride*	H_2CCC	propadienylidene	CH_3CH_3CO	acetone†
AlCl	aluminum chloride*	HCOOH	formic acid		
KCl	potassium chloride*	CH_2CO	ketene		
AlF	aluminum fluoride*†	HC_3N	cyanoacetylene	HC_9N	cyano-octa-tetra-yne
NH	nitrogen hydride	CH_2CN	cyanomethyl		

Table from previous slide continued

SiN	*	NH_2CN	cyanamide		
		CH_2NH	methanimine	$HC_{11}N$	cyano-deca-penta-yne
H_2D^+	†			CH_4	methane
C_2H	ethynyl			SiH_4	silane*
CH_2	methylene†			C_4Si	*
HCN	hydrogen cyanide			C_5	pentatomic carbon*
HNC	hydrogen isocyanide	C_5H	pentynylidyne	HCCNC	isocyanoacetylene
HCO	formyl	C_2H_4	ethylene*		
HCO^+	formyl ion	H_2CCCC	butatrienylidene		
HOC^+	isoformyl ion†	CH_3OH	methanol		
N_2H^+	protonated nitrogen	CH_3CN	methyl cyanide		
HNO	nitroxyl	CH_3NC	methyl isocyanide		
H_2O	water	CH_3SH	methyl mercaptan		
HCS^+	thioformyl ion	NH_2CHO	formamide		
H_2S	hydrogen sulfide	HC_3HO	propynal		
OCS	carbonyl sulfide				
SO_2	sulfur dioxide				
SiC_2	silicon dicarbide*				
C_2O	dicarbon monoxide				
C_3	triatomic carbon*				
C_2S					

[a] As of July 1992. Reported but doubtful, unconfirmed, or rejected: CO^+, CS^+, NaOH, NH_2CH_2COOH, CH_2CH_2O.

* Detected in circumstellar envelopes only.

† Tentative.

Interstellar chemistry: Photodissociation regions

UV radiation of mass-rich, early-type stars evaporates grains and dissociates molecules.

The “elephant trunks” hide condensations of newly forming stars. These clouds are denser and therefore resist the evaporation and dissociation longer.

Schema of a photodissociation region

Lequeux J., “The interstellar medium”, Springer 2005

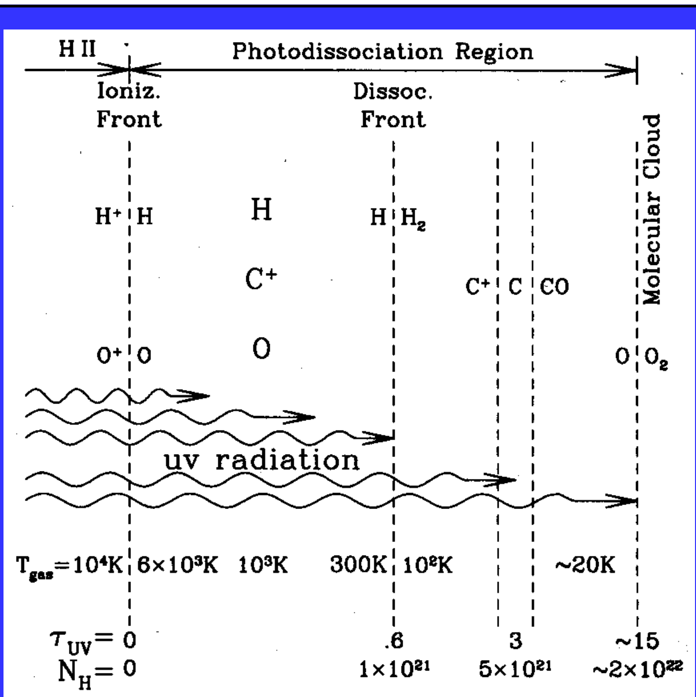

cm^2

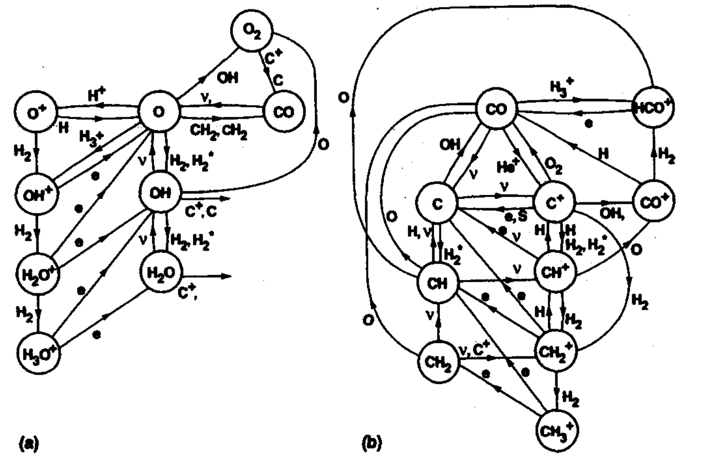

Fig. 10.2. The most important chemical reactions in photodissociation regions: (a) carbon chemistry; (b) oxygen chemistry. Compare to Figs. 9.2 and 9.3. Reproduced from Sternberg & Dalgarno [495], with the permission of the AAS.

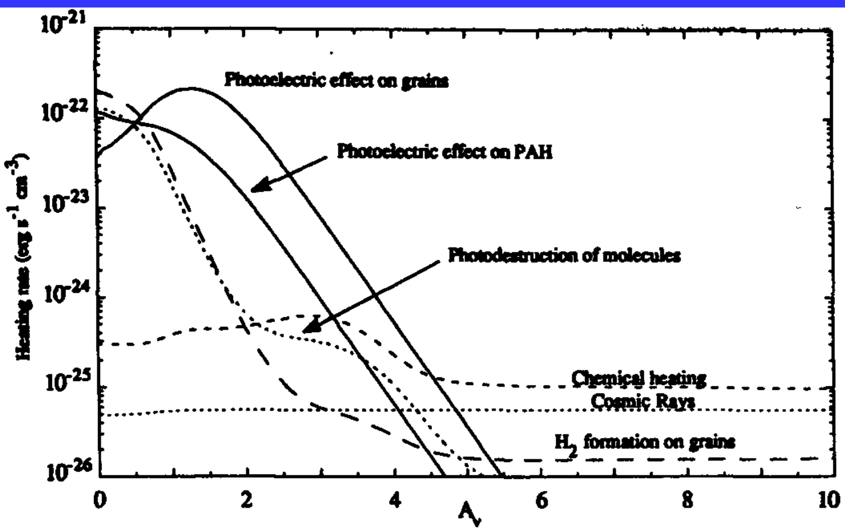

Av: visual extinction in magnitudes

Cloud collapse:

Force balance: pressure and centrifugal force versus gravitation.

Virial theorem: Multiply the equation of motion with the radius vector.
"Virial" = torque = Drehmoment
see J. Lequeux "The interstellar medium", Springer 2003, Chap. 14.

In the absence of external pressure $E_{Grav} = -2E_{Kin}$

Jeans mass M_J:

$$M_J \approx \left(\frac{kT}{G\mu_a m_{amu}}\right)^{3/2} \frac{1}{\sqrt{\rho}}.$$

The less dense the object is the more massive it must be to collapse.
Examples: galaxies, star clusters, stars, planets.
The cooler the object the easier it collapses.
$n > 10^{-11}$ g cm^{-3} and T=10K needed to form a Jupiter size planet. This density is much larger than that observed in interstellar clouds .

Gravitational collapse may be triggered by supernova explosion or a galactic density wave.

Galaxy NGC 1097

observed with 8.2 m Melipal Unit telescope of the VLT, ESO.

Note the bright regions of young stars and the dust lanes along the spiral arms of the galaxy.

Collapse of molecular cloud cores and star formation

Free fall time scale: $t_{ff} = \left(\frac{3\pi}{32G\rho}\right)^{1/2}$ For the Sun it is about 30 minutes.

Clumps are densest near their centers, collapse is inside-out.
Angular momentum conversation leads to spin-up of the cloud, may cause the collapse to stop and to fragment the cloud. Therefore most often multiple stellar systems form.

Virtually all single stars and many multiple stars are surrounded by a flat disk during formation. The mass collects in the central star and the angular momentum in the disk.

In solar system 99.8% of the mass is in the central star and 98% of the angular momentum is in planetary orbits.

Temperature and density rise during collapse. Cloud becomes opaque, pressure builds up, D is burnt into He. When D is exhausted, star shrinks and heats further up, ^{1}H fusion starts.

Early phases of star formation can be observed in the microwave range, which presently is a very active part of research. Later the star becomes visible in the IR wavelength range.

Early phases of protostars

André, Ph.: "The initial conditions for protostellar collapse: Observational constraints", in Star formation and the physics of young stars, J Bouvier and J.-P. Zahn (eds.) EAS Publication Series, Vol 2., 2002

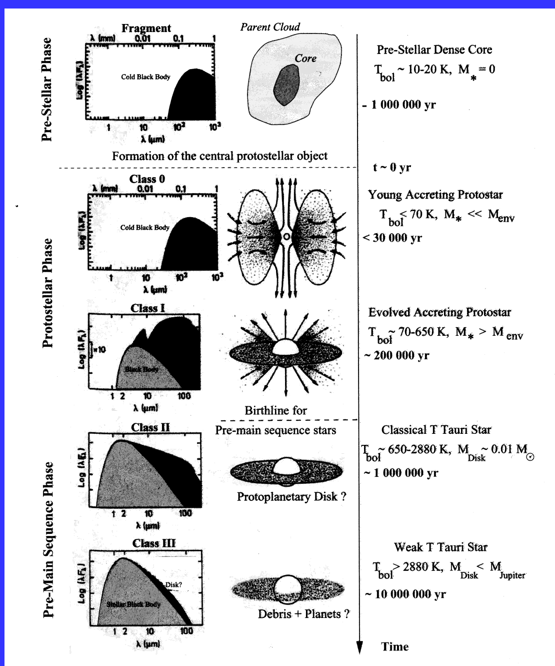

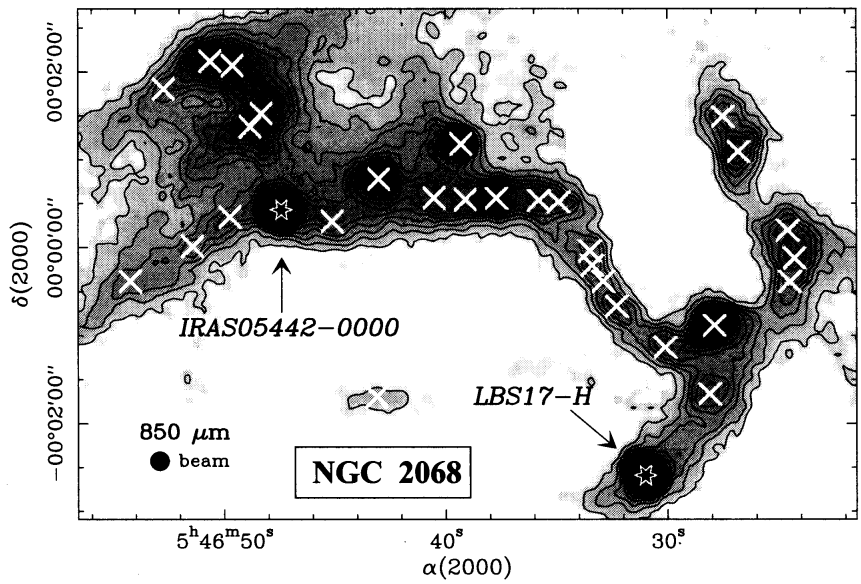

Protocluster NGC 2068: SCUBA 850μm dust continuum map shows 30 condensations. Field: 1 pc x 0.7 pc

Rotating protostellar disk DM Tau, obserded in millimeter range and presented here as three-dimensional spectrum.
The system is well fitted by Keplerian rotation
$V \sim r^{-0.5\pm0.1}$
Radius 525AU,
Mass = 0.6-0.85 $M_{\odot}$
Mundy et al., in Mannings, et al. eds. “Protostars and Planets IV”, U.of Az. Press, 2000, 355-376.

Lower panel not shown.

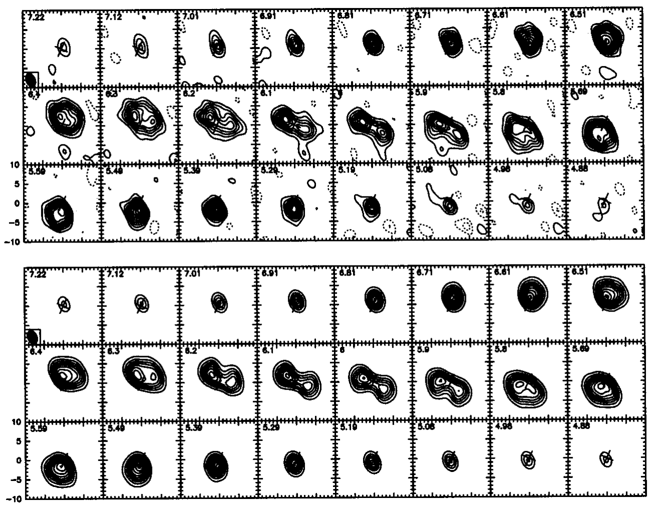

Figure 6. Images of the CO $J = 2$–1 emission, model, and residuals for the DM Tauri system from Guilloteau and Dutrey (1998). The upper set of panels shows the observed emission, with each panel labeled with velocity. The middle panels display the emission from the best-fitted model. The lower panels display the differences between the observations and the model. The angular resolution of the observations is 3.5 × 2.4″.

Orion Nebula

Note that HII region is *in front of dark cloud*!

see e.g. : Henbest N., Marten M., The New Astronomy, Cambridge 1983

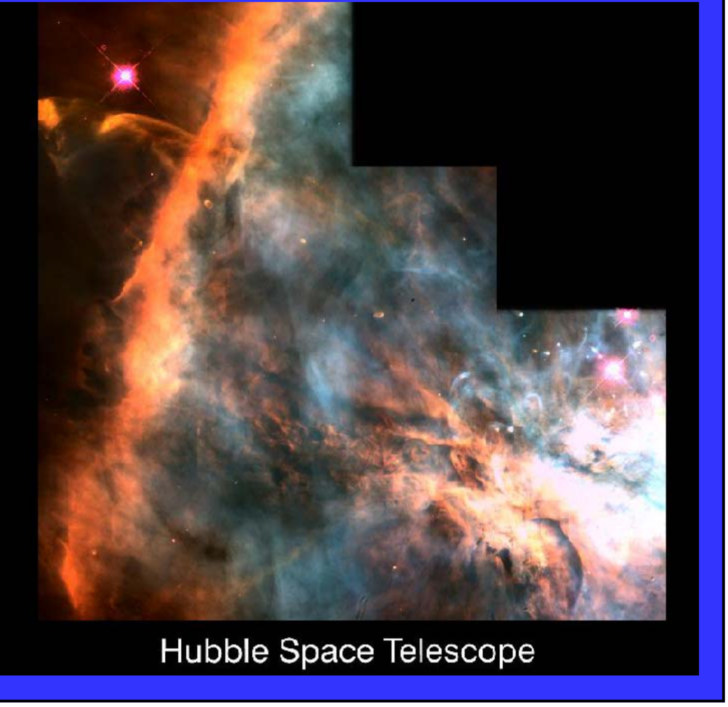

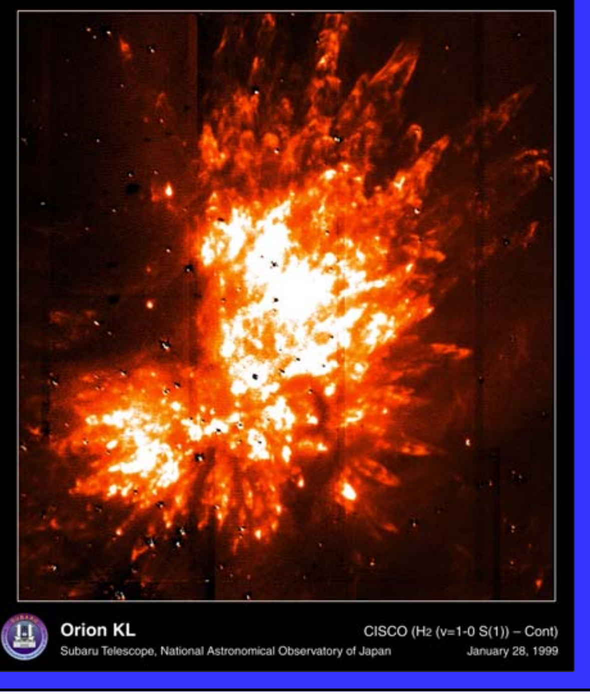

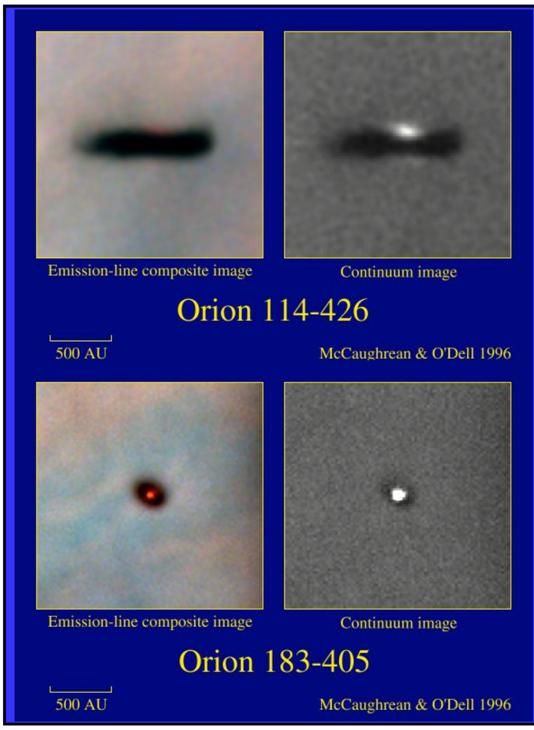

Hubble Space Telescope images of young circumstellar disks in the Orion Nebula. The lefthand panel of each image shows an emission-line composite, made by combining data from three narrow-band filters centred on bright emission lines from the nebula, namely [OIII] (blue), Halpha (green), and [NII] (red). The strong emission lines provide a bright background which reveals the circumstellar disks as silhouettes around their young stars. The righthand panel shows the corresponding continuum image taken through the medium bandwidth F547M filter. In these images, the central star shows up most clearly, and in the case of the edge-on disk, Orion 114-426, we also see faint reflection nebula above and below the plane of the silhouette disk.

Bally J., O'Dell C.R., McCaughrean M.J., 2000
Disks, microjets, windblown bubbles, and outflows in the Orion Nebula,
A.J. 119, 2919-2959

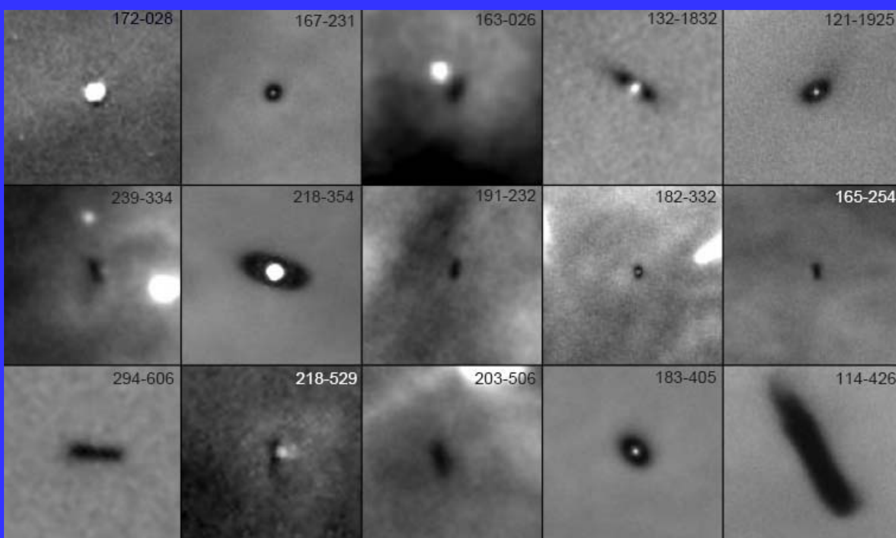

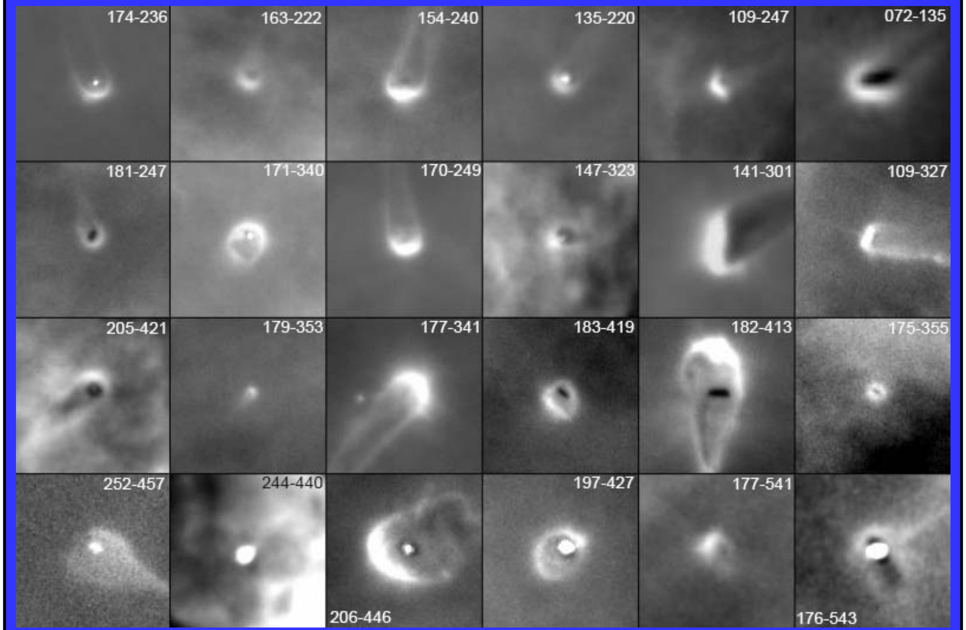

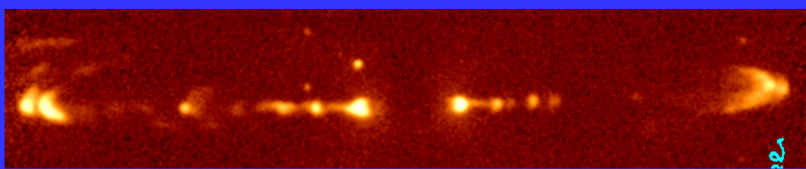

High-resolution deeper false-colour (v=1-0 S(1) line of molecular hydrogen at 2.122 microns) near-infrared image of the central knots and bowshocks in HH212. Continuum emission has not been subtracted. Data taken in November 1994 using the 256x256 pixel MAGIC infrared camera on the Calar Alto 3.5-m telescope in Spain. Field-of-view is approximately 55x85 arcsec, with the field rotated roughly 24 degrees west of north.

Credit: Mark McCaughrean (Astrophysikalisches Institut Potsdam), Hans Zinnecker (Astrophysikalisches Institut Potsdam), and John Rayner (University of Hawaii)

Star formation:

“Fundamental Astronomy”, Karttunen H. et al. eds., Springer 1987

Time scales again:
Thermal time scale:

$$t_t \approx \frac{0.5\,GM^2/R}{L} \approx \frac{(M/M_\odot)^2}{(R/R_\odot)(L/L_\odot)} \times 2 \times 10^7\,\mathrm{y}\,,$$

Dynamical (free fall) time scale

$$t_d = \frac{2\pi}{2}\sqrt{\frac{(R/2)^3}{GM}} \approx \sqrt{\frac{R^3}{GM}}\,.$$

Early evolution of a collapsing star:

in free-fall time
H_2, H, H^+ (10^4 K), He^+ (10^5 K).
Radius shrinks from 100 AU to 1/4AU.
Star is convective in its center.

Hayashi track: Location of fully convective stars in the HR diagram.

Further evolution on thermal time scale.
Star continues to contract, motion is downward. Then, as the energy input changes from gravitational to nuclear energy, the convective regime is steadily transferred into a radiative one, the steller surface becomes hotter and its luminosity increases.

12.2 The Contraction of Stars Towards the Main Sequence

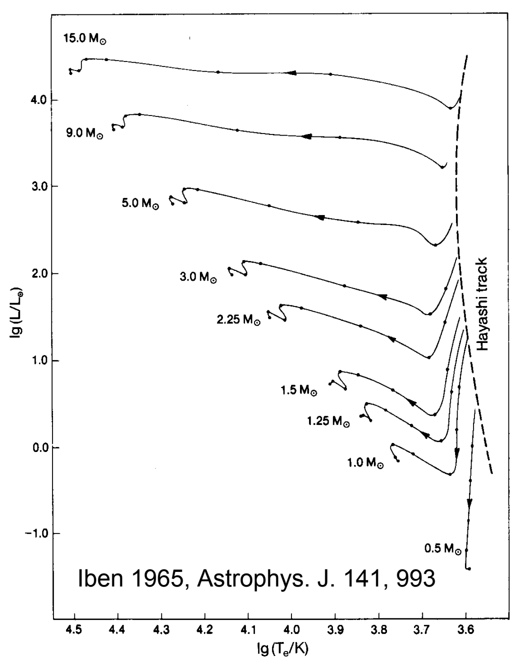

Iben 1965, Astrophys. J. 141, 993

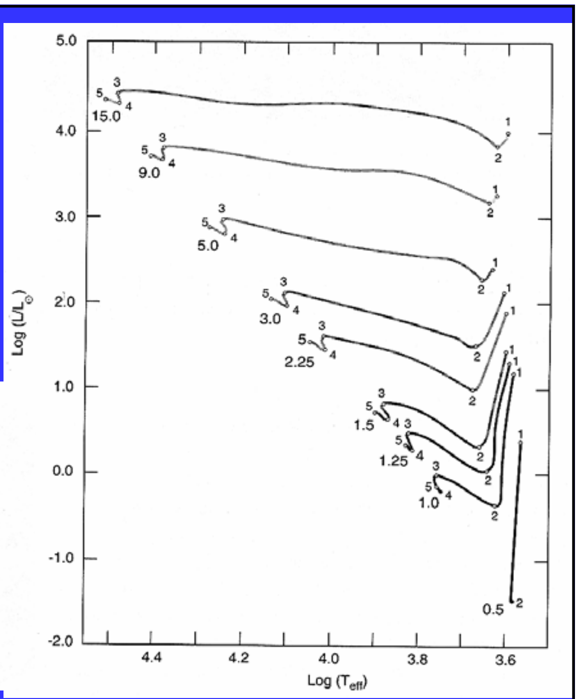

Table 8.1 Evolutionary lifetimes (years)

$M/M_\odot$	*1–2*	*2–3*	*3–4*	*4–5*
15	6.7(2)	2.6(4)	1.3(4)	6.0(3)
9	1.4(3)	7.8(4)	2.3(4)	1.8(4)
5	2.9(4)	2.8(5)	7.4(4)	6.8(4)
3	2.1(5)	1.0(6)	2.2(5)	2.8(5)
2.25	5.9(5)	2.2(6)	5.0(5)	6.7(5)
1.5	2.4(6)	6.3(6)	1.8(6)	3.0(6)
1.25	4.0(6)	1.0(7)	3.5(6)	1.0(7)
1.0	8.9(6)	1.6(7)	8.9(6)	1.6(7)
0.5	1.6(8)			

Note: powers of 10 are given in parentheses.

Early evolution of a collapsing star (continued):

A star of 15 solar masses condenses to the main sequence in 60000 years,
for a star with 0.1 solar masses the process takes hundreds of millions of years.

Very young stars (T Tauri stars) difficult to observe as they are enshrouded into dense clouds.
T Tauri stars have high Lithium content (central temperature not yet high enough to destroy Lithium).

Bonnor-Ebert-Sphere:

Equilibrium isothermal sphere of finite size with a fixed temperature and boundary pressure; such a configuration might be relevant to star formation if prestellar cloud cores when formed are nearly in equilibrium and in approximate pressure balance with a surrounding medium. For a fixed sound speed *c* and boundary pressure *P*, an isothermal sphere is unstable to collapse if its radius and mass exceed the critical values

$$R_{BE} = \frac{0.48\, c^2}{G^{1/2} P^{1/2}}, \quad M_{BE} = \frac{1.18\, c^4}{G^{3/2} P^{1/2}}$$ (Bonnor–Ebert sphere).

These results can be related to the Jeans length and mass discussed above by noting that in an isothermal medium the pressure and density are related by $P = \rho c^2$ (*c* is sound speed);
thus, R_{BE} and M_{BE} have the same dimensional form as the Jeans length and mass, but with smaller numerical coefficients that reflect the fact that a Bonnor–Ebert sphere contains only matter whose density is higher than the background density, while a region one Jeans length across also includes matter of lower density that may or may not collapse along with the denser material.

(R.B. Larson, The physics of star formation, Rep. Prog. Phys. 66, 1651-1697, 2003)

Calculation of collapse of "Bonnor-Ebert" sphere prior to reaching Hayashi-line by taking full account of supersonic compressible motion of the cloud gas, but assuming spherical symmetry and grey Eddington approximation.
Note that the initial star may be brighter as expected and therefore better observable.

r_τ radius where $\tau_{ROSS} = 2/3$ (photospheric radius)
thick line: $L = 4\pi r_\tau^2 \sigma T^4_{eff}$,
dashed line: $L = 4\pi r_\tau^2 \sigma T^4$,
dotted line: T at r_τ.

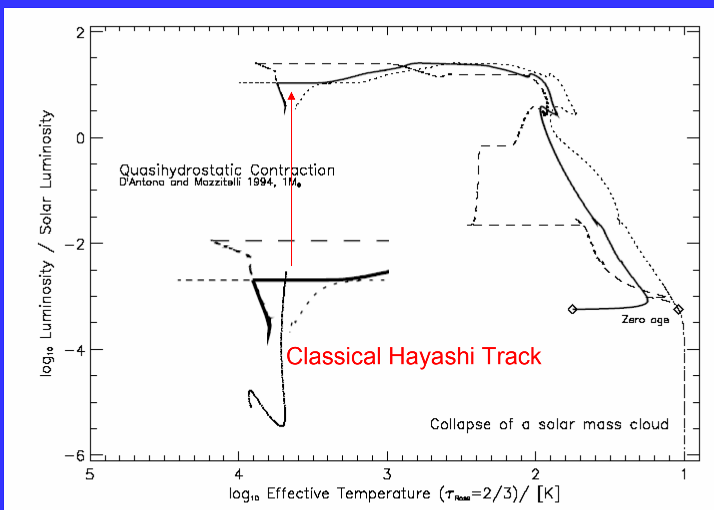

Wuchterl G., W.M.. Tscharnuter, A&A 398, 1081-1090 (2003)

(a) (b)

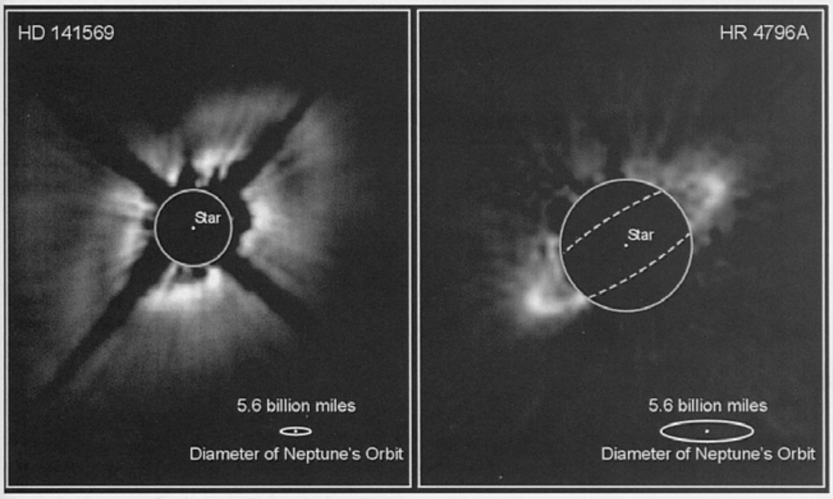

FIGURE 12.5 Coronographic images of disks around young stars. (a) A near-infrared image of a disk around the star HD 141569, located about 320 light-years away in the constellation Libra. A dark band separates a bright inner region of the ~750 AU wide disk from a fainter outer region. This band may be the result of the formation of a planet in the disk. (Courtesy: B. Smith and G. Schneider, HST/NASA) (b) A near-infrared image of a dust ring around the young ($\lesssim 10^7$ yr old) star HR 4796A. The ring, at a distance of ~40 AU from the central star, is less than 17 AU wide. The confinement of this ring suggests the presence of unseen planets in orbit around the star. In both cases a coronagraph was used to block off the light from the star. (Courtesy: E. Becklin and A. Weinberger, HST/NASA)

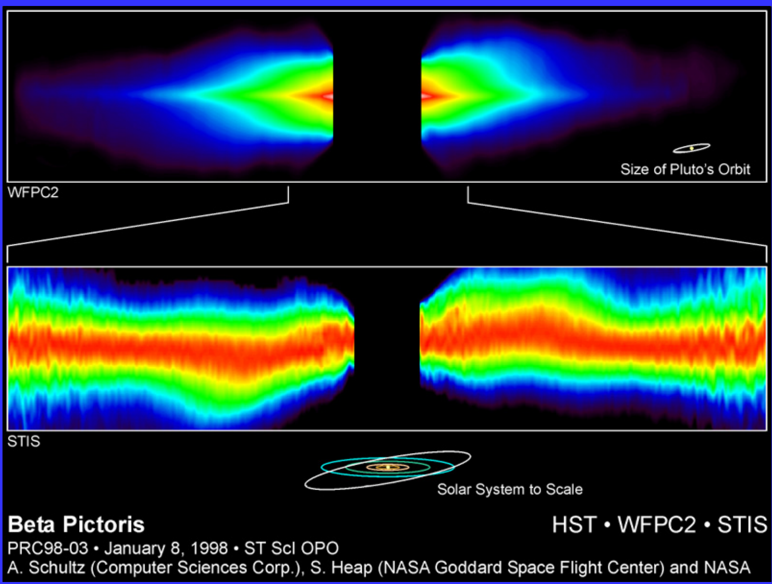

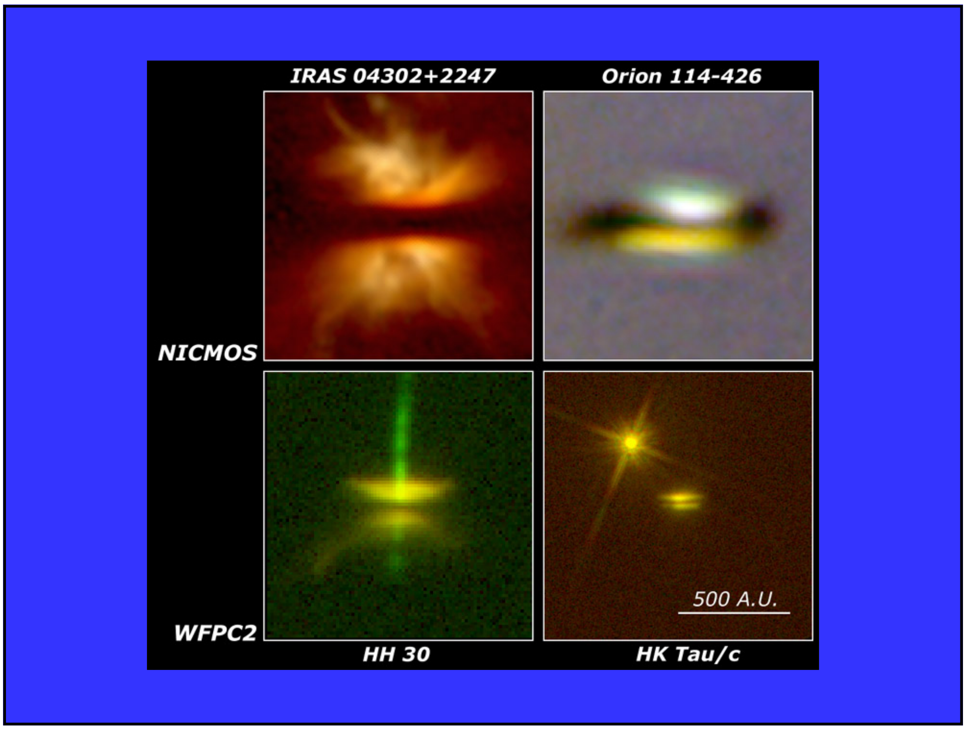
IRAS 04302+2247
Orion 114-426
NICMOS
WFPC2
500 A.U.
HH 30
HK Tau/c

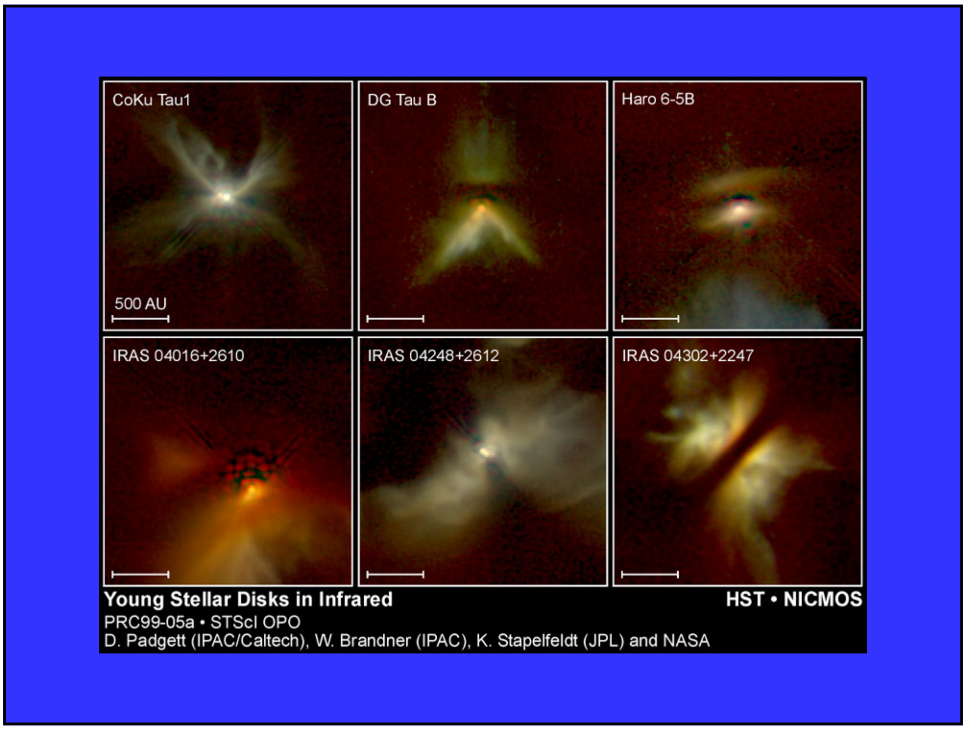
CoKu Tau1
DG Tau B
Haro 6-5B
500 AU
IRAS 04016+2610
IRAS 04248+2612
IRAS 04302+2247
Young Stellar Disks in Infrared
HST • NICMOS
PRC99-05a • STScI OPO
D. Padgett (IPAC/Caltech), W. Brandner (IPAC), K. Stapelfeldt (JPL) and NASA